ACS APPLIED MATERIALS & INTERFACES

Research Article

www.acsami.org

Design of Poly(Acrylonitrile)-Based Gel Electrolytes for High-Performance Lithium Ion Batteries

Shih-Hong Wang,[†] Ping-Lin Kuo,[†] Chien-Te Hsieh,*[,‡] and Hsisheng Teng*[,†,§]

[†]Department of Chemical Engineering and Research Center for Energy Technology and Strategy, National Cheng Kung University, Tainan 70101, Taiwan

[‡]Department of Chemical Engineering and Materials Science, Yuan Ze Fuel Cell Center, Yuan Ze University, Taoyuan 32023, Taiwan

[§]Center for Micro/Nano Science and Technology, National Cheng Kung University, Tainan 70101, Taiwan

Supporting Information

ABSTRACT: The use of polyacrylonitrile (PAN) as a host for gel polymer electrolytes (GPEs) commonly produces a strong dipole−dipole interaction with the polymer. This study presents a strategy for the application of PAN in GPEs for the production of high performance lithium ion batteries. The resulting gel electrolyte GPE-AVM comprises a poly(acrylonitrile-*co*-vinyl acetate) copolymer blending poly(methyl methacrylate) as a host, which is swelled using a liquid electrolyte (LE) of 1 M $LiPF_6$ in carbonate solvent. Vinyl acetate and methacrylate groups segregate the PAN chains in the GPE, which produces high ionic conductivity (3.5×10^{-3} S cm^{-1} at 30 °C) and a wide electrochemical voltage range (>6.5 V) as well as an excellent Li^+ transference number of 0.6. This study includes GPE-AVM in a full-cell battery comprising a $LiFePO_4$ cathode and graphite anode to promote ion motion, which reduced resistance in the battery by 39% and increased the specific power by 110%, relative to the performance of batteries based on LE. The proposed GPE-based battery has a capacity of 140 mAh g^{-1} at a discharge rate of 0.1 C and is able to deliver 67 mAh g^{-1} of electricity at 17 C. The proposed GPE-AVM provides a robust interface with the electrodes in full-cell batteries, resulting in 93% capacity retention after 100 charge−discharge cycles at 17 C and 63% retention after 1000 cycles.

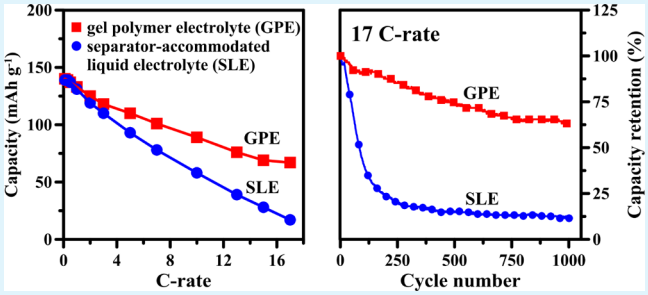

KEYWORDS: *gel polymer electrolyte, lithium ion battery, poly(acrylonitrile), poly(methyl methacrylate), $LiFePO_4$ electrode*

1. INTRODUCTION

Rapid developments in portable electronic devices and electric vehicles (EVs) have increased demand for high performance energy storage systems, which has fueled widespread research into the development of high-performance lithium ion batteries (LIBs).[1] The composition of electrolytes affects the chemical stability and active voltage range of LIBs, while with defected cell sealing or over many years of operation the leakage or evaporation of solvent from the electrolyte solution limits the operating life. One solution to these problems lies in the development of gel polymer electrolytes (GPEs), which can provide ionic conductivity comparable to, or even superior to, that of liquid electrolytes.

Researchers have developed several polymer hosts of GPEs for LIB applications. These hosts include poly(ethylene oxide),[2] poly(vinylidene fluoride) (PVDF),[3,4] poly(vinylidene fluoride-*co*-hexafluoropropylene),[5−7] poly(urethane),[8] poly(acrylonitrile) (PAN),[9] poly(methyl methacrylate) (PMMA),[10−12] poly(vinyl chloride),[13] and polyimide.[14] Table 1 presents a performance summary of full cells assembled using GPEs of various compositions.[15−27] Most of these batteries had either low rate capacity (<10 C) and, therefore, lacked the power required to switch on EVs, or exhibited poor capacity retention during cycling. The effectiveness with which polymers trap solvent molecules and dissociate solvated ion clusters largely determines the power performance of GPE-based LIBs.[28] Polymer functionalities designed specifically to facilitate Li^+-ion motion are able to suppress electrode polarization and reduce transport resistance.[29] In addition, a strong dipole−dipole interaction between polymer functional groups and solvent molecules could be expected to stabilize the solvent and may be applied as a means to extend the operating life.[30]

Among the aforementioned polymer hosts, PAN exhibits excellent ion-solvating ability, thermal stability, material processability, flame resistance, resistance to oxidative degradation, electrochemical stability, and compatibility with lithium electrodes.[31,32] The −CN groups in PAN interact with the −CO groups of carbonate solvent molecules and Li^+ ions without a notable degradation in mechanical properties.[33,34] However, PAN suffers from low solvent-trapping ability that can cause leakage of the GPEs. Crystallization associated with the polar interaction of adjacent −CN groups in the main PAN

Received: August 13, 2014
Accepted: October 20, 2014
Published: October 20, 2014

Table 1. Capacity Values and Cycle Lives of Full-Cell Lithium Ion Batteries Assembled with Different Electrolytes

GPE composition (polymer/electrolyte)[a]	anode|cathode[b]	capacity (mAh g^{-1})	cycling retention	ref
PMMA/PVC/$LiPF_6$-EC-DMC	graphite|LCO	133 @ 1 C 114 @ 5 C	98%, 100 cycles @ 0.5 C	12
PAN/$LiPF_6$-EC-DMC-DEC	graphite|LCO	113 @ 1/20 C	86%, 30 cycles @ 0.5 C	15
PVdF-CTFE/$LiPF_6$-EC-DMC	Sn−C|LNM	10 @ 1/3 C 60 @ 3 C		16
P(VdF-HFP)-SiO_2/$LiPF_6$-EC-DEC	graphite|LCO		93%, 100 cycles @ 0.5 C	17
α-CD(PMMA)/$LiClO_4$-EC-PC	graphite|LCO	130 @ 0.5 C 138 @ 0.1 C	98%, 20 cycles @ 0.1 C	18
P(EO-EM-AGE)/$LiPF_6$-EC-PC-DMC	graphite|LNCM	128 @ 0.1C 60 @ 5 C	95%, 300 cycles @ 0.5 C	19
P(OEGMA-BnMA)/$LiPF_6$-EC-DMC	graphite|LFP	122 @ 0.1 C 25 @ 5 C	91%, 50 cycles @ 0.5 C	20
	Graphite|LNCM	148 @ 0.1 C 119 @ 1 C 40 @ 5 C	93%, 200 cycles @ 0.5 C	
P(PEGMEMA-BMI)/$LiPF_6$-EC-PC-DEC	MCMB|LCO		94%, 100 cycles @ 0.2 C	21
TMPTMA/$LiPF_6$-EC-EMC-DMC	graphite|LCO	135 @ 0.1 C 110 @ 1 C	83%, 100 cycles @ 0.2 C	22
D4-ep(n = 1)-PVPS/$LiPF_6$-EC-DMC	graphite|LCO	130 @ 0.1 C 61 @ 3 C	97%, 200 cycles @ 1 C	23
PI/$LiPF_6$-EC-EMC	graphite|LCO	157 @ 0.2 C 77 @ 2 C	76%, 100 cycles @ 0.5 C	24
PI/$LiPF_6$-EC-FEC-EMC-DMC	graphite|LCO	180 @ 0.2 C 80 @ 2 C	85%, 50 cycles @ 0.5 C	25
PI/$LiPF_6$-EC-EMC	graphite|LCO	158 @ 0.2 C 119 @ 2 C	85%, 50 cycles @ 0.5 C	26
P(EO-PO)/ $LiPF_6$-EC-DMC-DEC	graphite|LFP	125 @ 0.5 C 88 @ 5 C 12 @ 17 C	77%, 450 cycles @ 1 C	27
PAVM/$LiPF_6$-EC-DEC-DMC	graphite|LFP	140 @ 0.1 C 118 @ 3 C 67 @ 17 C	93%, 100 cycles @ 17 C 63%,1000 cycles @ 17 C	this work

[a]$LiPF_6$, lithium hexafluorophosphate; EC, ethylene carbonate; DMC, dimethyl carbonate; DEC, diethyl carbonate; CTFE, chlorotrifluoroethylene; α-CD(PMMA), α-cyclodextrin(poly(methyl methacrylate)); $LiClO_4$, lithium perchlorate; PC, propylene carbonate; P(EO-EM-AGE), poly(ethylene oxide-2-(2-methoxyethoxy) ethyl glycidyl ether-allyl glycidyl ether); P(OEGMA-BnMA), poly(oligo (ethylene glycol) methyl ether methacrylate-benzyl methacrylate); P(PEGMEMA-BMI), poly(poly(ethylene glycol) methyl ether methacrylate-bismaleimide); TMPTMA, trimethylolpropane trimethyl acrylate; EMC, ethyl methyl carbonate; D4-ep(n = 1), 2,4,6,8-tetrakis(3-((oxiran-2-yl) methoxy) propyl)-2,4,6,8-tetramethyl-1,3,5,7,2,4,6,8-tetraoxatetrasilocane; PVPS, P(2-vinylpyridine-styrene); PI, polyimide; FEC, fluoroethylene carbonate; P(EO-PO), poly(ethylene oxide-*co*-propylene oxide). [b]LCO, $LiCoO_2$; LNM, $LiNi_{0.5}Mn_{0.5}O_4$; LNCM, $Li_x(Ni_{1/3}Co_{1/3}Mn_{1/3})_{(2-x)}O_2$; LFP, $LiFePO_4$.

chains also increases the resistance to the transport of Li^+ ions.[35] Copolymerization with other polymers has been used to overcome the shortcomings of PAN.[36] The addition of poly(vinyl acetate) (PVAc) in PAN to form poly-(acrylonitrile-vinyl acetate) (PAV) reduces the crystallinity of the polymer and enhances mechanical stability.[37] Vinyl acetate also enhances the adhesion between GPEs and electrode materials.[38]

This study used PAV and PMMA-incorporated PAV (i.e., PAVM) as polymer hosts for GPEs. The introduction of PMMA also improves ion transfer at the electrolyte-electrode interface and reduces the brittleness of polymers containing PAN.[39−41] This study employed electrospinning for the preparation of polymer-host films comprising fine fibers with diameters in the range of 10 nm−10 μm.[8] The electrospun films provide a large exposed area over which to incorporate the Li-ion electrolyte solution into the polymer framework, thereby assuring complete segregation of the polymer chains in the GPEs. GPE synthesized using PAVM enhances the performance of full-cell graphite|electrolyte|$LiFePO_4$ batteries by lowering resistance, accelerating discharge performance, and extending the cycle lifespan.

2. EXPERIMENTAL SECTION

2.1. Preparation of Polymer Host of GPEs. This study prepared polymer host PAVM through the addition of PMMA (Aldrich, USA; weight-average molecular weight (M_w) = 15 000 g mol^{-1}) to a solution comprising 7 wt % PAV (Tong-Hwa, Taiwan; M_w = 500 000 g mol^{-1}, acrylonitrile/vinyl acetate ratio =92/8) dissolved in dimethylacetamide. The mixture, with a PMMA/PAV mass ratio of 1/10, was magnetically stirred at 70 °C for 12 h. The resulting polymer solution was used as a feed for the electrospinning synthesis of PAVM on aluminum foil. Electrospinning was conducted using a polymer solution feed rate of 0.7 mL h^{-1} and an applied voltage of 15 kV, with a distance of 15 cm between the tip of a nozzle and collector. After collecting electrospun films (average thickness of 50−200 μm), they were dried under vacuum on thin aluminum foil at 60 °C for 12 h. Electrospun PAV films were also prepared using the same process as that used for the PAVM, except for the addition of PMMA.

The PAVM and PAV films were soaked in a liquid electrolyte solution (LE) of 1 M $LiPF_6$ dissolved in ethylene carbonate/dimethyl

carbonate/diethyl carbonate (EC/DMC/DEC; 1:1:1 by volume) in an argon environment for 24 h to trap the LE solution in the polymer network for the formation of GPE films.

2.2. Electrode Preparation and Cell Assembly. The cathode comprised 80 wt % $LiFePO_4$ (BTR New Energy Materials, China), 10 wt % PVDF (Aldrich, USA; M_w = 534 000 g mol^{-1}), and 10 wt % carbon black super-P (Taiwan Maxwave Co., Taiwan). A slurry of these materials was prepared in *N*-methyl pyrrolidone (NMP; Aldrich, USA) for the coating of aluminum foil using a doctor-blade. After evaporating the solvent, disks of 1.327 cm^2 in area were obtained by punching the coated foil followed by drying at 80 °C under vacuum for 12 h. The cathodes were then roll pressed to improve particulate contact and foil adhesion. The resulting electrodes had a thickness of 60−70 μm and an apparent density of 1.1 g cm^{-3}. The anode was prepared in the same manner as the cathode using 92 wt % mesophase pitch-derived graphite (China Steel Chemical Co., Taiwan), 6 wt % PVDF, and 2 wt % super-P with copper foil as the substrate. The thickness of the anode ranged from 40 to 50 μm with an apparent density of 1.1 g cm^{-3}. Full-cell LIBs were assembled by sandwiching the GPEs between a graphite anode and a $LiFePO_4$ cathode and then vacuum sealing the battery in a coin cell. All cell assembly was performed in a glovebox filled with argon gas.

2.3. Measurements. The surface morphology of the PAVM and PAV films and GPEs were examined using scanning electron microscopy (SEM; JEOL JSM-6700F, Japan). Raman spectra of the specimens were recorded at room temperature at a resolution of 4 cm^{-1} using a Bayspec Raman spectrometer (USA) with a laser line of 1064 nm using the Lorentzian function to deconvolute bands into constituent peaks. The ionic conductivity of the GPEs was determined using AC impedance spectroscopy (Zahner-Elecktrik IM6e, Germany) at temperatures of −40 to 90 °C. Two stainless-steel (SS) electrodes were used to sandwich the GPEs for measurement of impedance, which were conducted at 0 V with an AC potential amplitude of 5 mV and frequency range of 0.1 Hz to 1 kHz. The electrochemical stability of the GPEs was analyzed using linear voltage scans on SSlelectrolytel Li cells at 5 mV s^{-1}. Galvanostatic charge and discharge cycling tests were conducted on full-cell graphitelelectrolytelLiFePO$_4$ batteries between 2.0 and 3.8 V using battery test equipment (Acutech System BAT-750, Taiwan). Resistance at the electrolyte/electrode interface was measured using the impedance response of the full-cell batteries at frequencies ranging from 0.1 Hz to 100 kHz under various applied voltages. All electrochemical measurements were conducted at 25 °C. The electrochemical performance of the GPEs was compared with a commercial separator (Celgard M824, USA; 12 μm thick) swelled using LE (1 M $LiPF_6$ EC/DMC/DEC solution). The LE that was accommodated by the Celgard separator was designated as SLE in the following discussion.

3. RESULTS AND DISCUSSION

3.1. Preparation and Characterization of GPEs. Figure 1 presents SEM images of electrospun PAV and PAVM membranes, both of which consist of nanofibers 130 ± 70 nm in diameter. The fibers are interlaid to form a 3D network with fully interconnected interstitial pores between the fibers. These porous membranes can be evenly swollen by electrolyte solutions and offer connected channels for ion transport. Soaking the PAV and PAVM membranes in an LE comprising 1 M $LiPF_6$ dissolved in EC/DMC/DEC solution (1:1:1 by volume) yielded GPE films.

Figure 2 illustrates the electrolyte uptake of the PAV and PAVM membranes as a function of soaking time. After 30 min, the membranes reached saturation in the absorption of LE; total uptake was 2.2 and 2.6 times the masses of the PAV and PAVM, respectively. It is possible that the introduction of PMMA into the PAV polymer framework segregated the PAN chains in PAV, thereby increasing the availability of solvent molecules. Figure 2 also presents the volumes of LE absorbed

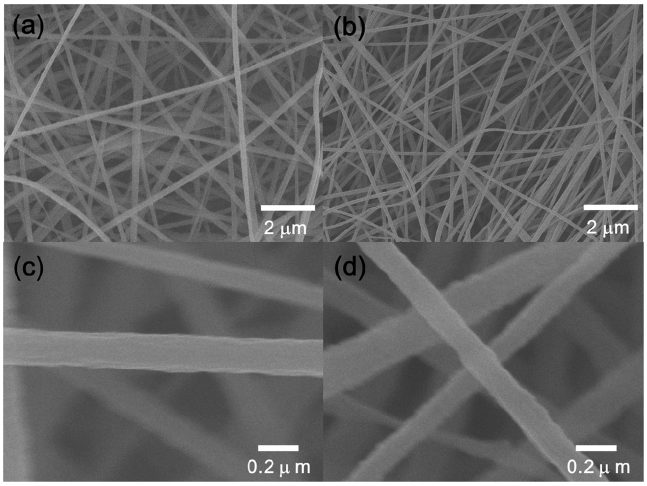

Figure 1. SEM images of electrospun polymer membranes: (a, c) PAV and (b, d) PAVM.

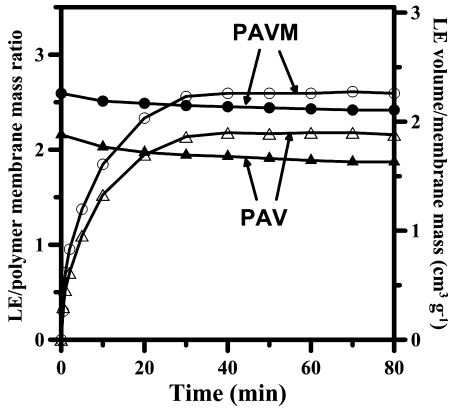

Figure 2. LE-uptake behavior (hollow symbols) when soaking the PAVM and PAV membranes in the LE solution (1 M $LiPF_6$-EC/DMC/DEC) and LE-leakage behavior (solid symbols) when pressing the LE-saturated PAVM and PAV with a load of 9.8 N cm^{-2}.

per unit mass of the membranes. The LE volumes filled the voids of the electrospun membranes to coagulate the composites into gels. Scheme 1 illustrates the process involved in the integration of PMMA into the PAV framework for the formation of PAVM. The segregation of PAV chains by polymeric chains of PMMA reduces the likelihood of crystallization in PAN-based polymers and creates free volume for the transport of lithium ions. PMMA is isomeric with poly(vinyl acetate) in PAV, which gives it greater freedom with regard to segmental motion because the ester side groups in the acrylate are less of a hindrance to polymer-chain rotation compared to acetate.[42]

Figure 2 also depicts the leakage behavior of LE-saturated polymer membranes that were subjected to a pressing load of 9.8 N cm^{-1}. Leakage loss stabilized after 60 min, at which point the masses of the remaining LE were 1.9 and 2.4 times the masses of the PAV and PAVM, respectively. We then used stabilized LE-loaded PAV and PAVM films as the gel electrolytes, that is, GPE-AV and GPE-AVM, respectively, in subsequent cell assembly and analysis.

Figure 3a and b presents top-view photographs of the PAV and PAVM membranes (1.8 cm in diameter and 60 μm thick), which are flexible, white, and completely opaque to light. The GPE-AV and GPE-AVM gel electrolytes (formed by incorpo-

Scheme 1. Conceptual Illustration of the Polymer Frameworks of PAV and PAVM[a]

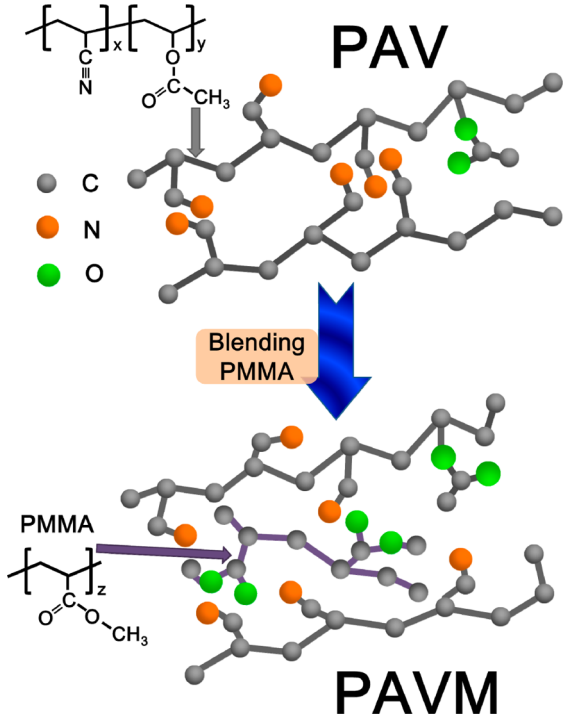

[a]In PAVM, PMMA chains segregate the PAN segments in PAV to reduce the crystallization tendency of PAN and create free volume.

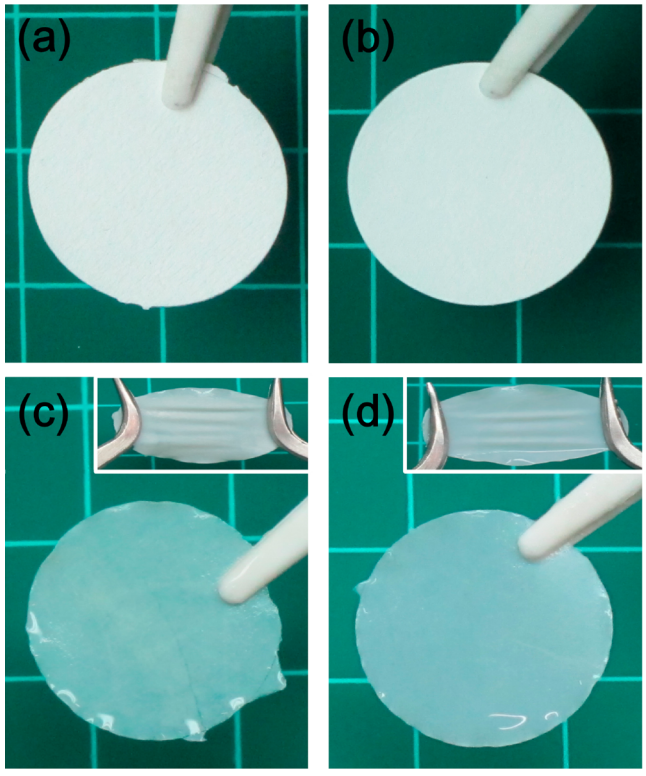

Figure 3. Top-view photographs of the (a) PAV membrane, (b) PAVM membrane, (c) GPE-AV, and (d) GPE-AVM. The insets of panels c and d show the tensile test of GPE-AV and GPE-AVM.

rating LE into polymer membranes) appeared homogeneous, mechanically stable, and translucent, as shown in Figure 3c and d. The insets of Figure 3c and d illustrate the elastic nature of the GPE films, which did not break when subjected to stretching.

Figure 4 presents the Raman spectra of SLE and GPEs in various wavenumber regions. The strong band at 700−760

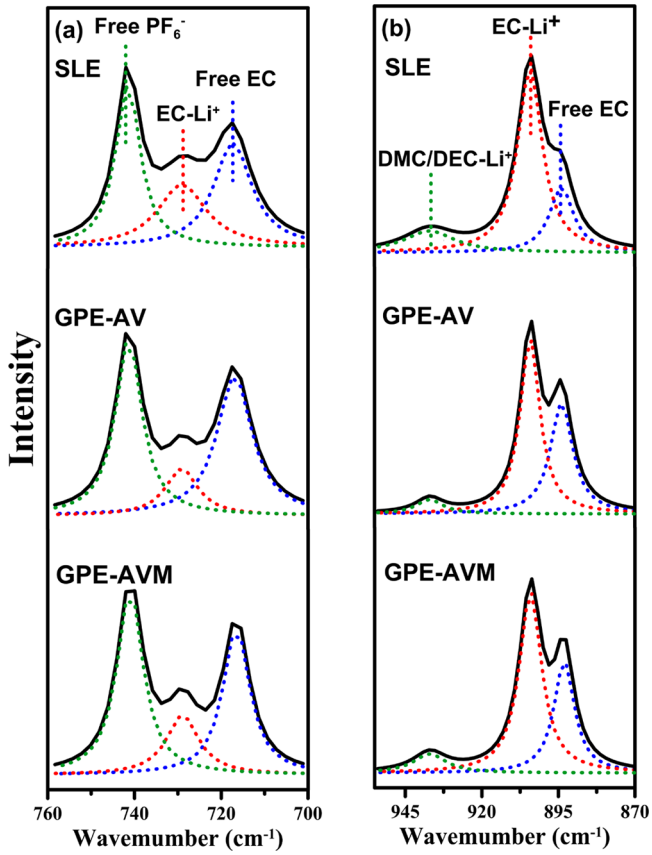

Figure 4. Raman spectra (solid lines) of SLE, GPE-AV, and GPE-AVM and the constituting peaks obtained after spectrum deconvolution (dotted lines) in difference wavenumber regimes: (a) 700−760 and (b) 870−955 cm^{-1}.

cm^{-1} (Figure 4a) corresponds to ring bending modes of free-EC and Li^+-associated EC (EC-Li^+) at 717 and 726 cm^{-1}, respectively, and the symmetric vibration of free PF_6^- at 741 cm^{-1}.[43] We employed Lorentzian curve fitting to deconvolute this band into its constituent peaks (dotted lines). Because of the high dielectric constant of EC (approximately 90), the $LiPF_6$ salt completely dissociated from the electrolytes, such that the peak of PF_6^- could be used as a reference for the evaluation of the relative intensities associated with other peaks or bands in the Raman spectra.[44−47] The (free-EC + EC-Li^+)/(free-PF_6^-) peak-area ratios for SLE, GPE-AV, and GPE-AVM were 1.7, 1.3, and 1.1, respectively. The ratios of the GPEs were smaller than that of SLE, indicating that some EC molecules were associated with polymer chains in the GPEs.[43,48,49] GPE-AVM, which exhibited the lowest EC ring-bending intensity, demonstrated the ability to entrap solvent molecules in the polymer framework.

Figure 4b presents the Raman 870−955 cm^{-1} region, which includes contributions from the symmetric ring breathing of free-EC and EC-Li^+ at 894 and 904 cm^{-1}, respectively as well as the O−CH_3 stretching of DEC/DMC-Li^+ at 937 cm^{-1}.[43] No signal for free DEC/DMC (920 cm^{-1}) was observed in the

dx.doi.org/10.1021/am505448a | ACS Appl. Mater. Interfaces 2014, 6, 19360−19370

spectra, indicating that the DEC and DMC molecules were completely associated with Li^+ ions or polymer chains. The (EC-Li^+ + DEC/DMC-Li^+)/(free-EC) peak-area ratios for SLE, GPE-AV, and GPE-AVM were 4.1, 1.6, and 1.6, respectively. The smaller ratios associated with the GPEs indicate that the Li^+-solvent complexes interacted with the polymer chains in the GPEs, thereby lowering their Raman signals. The interaction between solvent-solvated Li^+ ions and polymer chains may have facilitated the transport of Li^+ ions through GPEs via the segmental motion of polymer chains.

3.2. Ionic Conductivity of GPEs. This study employed the AC impedance method for the analysis of ionic conductivity in GPEs and SLE at various temperatures. Figure S1 of the Supporting Information presents data related to the impedance of SLE, GPE-AV, and GPE-AVM electrolytes at temperatures ranging from 20 to 90 °C. The GPEs had smaller real-component impedance values (i.e., Z' values) than SLE, indicating that the polymer framework in the GPEs was more efficient than the commercial separator membrane (Celgard-M824) in facilitating ion transport for SLE. The ionic conductivity of the electrolytes was determined as follows:

$$\sigma = R_I^{-1} S^{-1} d \quad (1)$$

where σ represents ionic conductivity, R_I is the real axis intercept in the impedance Nyquist plot, S is the geometric area of the electrolyte-electrode interface, and d is the distance between the two electrodes.[50]

Figure 5 presents a summary of an Arrhenius plot showing the ionic conductivity in the electrolyte at temperatures between −40 and 90 °C. The GPEs were more ion-conductive than SLE. For example, the following ionic conductivity values were obtained at 30 °C: 3.5×10^{-3} (GPE-AVM), 2.5×10^{-3} (GPE-AV), and 5.1×10^{-4} S cm^{-1} (SLE). The condition of the free volume around the polymer chains governed the overall mobility of ions and polymer chains, and therefore had a controlling effect on ionic conductivity.[51,52] The lower conductivity of SLE can be attributed to the use of a Celgard separator, which exhibits a resistance that is inherent to the electrolyte system and which was not designed to entrap electrolyte solution for free volume formation.[53] The LE uptake in SLE was only 0.4 time the mass of the Celgard membrane. The higher conductivity of GPE-AVM relative to that of GPE-AV is attributable to the introduction of PMMA, which segregated the PAN segments and created interstitial space for ion transport.[54,55] Providing interstitial space also increases polymer-chain motion, thereby facilitating the transport of ions.[56,57]

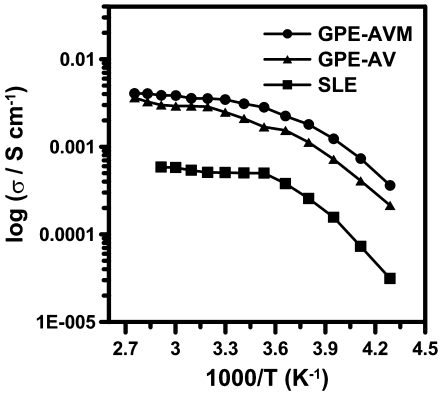

Figure 5. Ionic conductivities of the GPEs and SLE determined from the impedance analysis at temperatures of −40 to 90 °C (see Figure S1 of the Supporting Information).

As shown in Figure 5, the temperature dependence of SLE conductivity can be divided into two temperature regimes with a transition near 10 °C. Variations in conductivity were shown to obey the Arrhenius equation ($\sigma = \sigma_0 \exp(-E_a/RT)$, in which σ_0 is the frequency factor, E_a is the activation energy, R is the gas constant, and T is absolute temperature),[58,59] with activation energies of 2 and 31 kJ mol^{-1} for the high and low temperature regimes, respectively. The large E_a in the low-temperature regime indicates that crystallization of the carbonate solvents influenced the conductivity of SLE. The conductivity curves of the GPEs did not fit the Arrhenius equation, but rather the Vogel−Tamman−Fulcher (VTF) equation ($\sigma = AT^{-1/2} \exp[-E_0/R(T-T_0)]$, in which A is a constant proportional to the number of carrier ions, E_0 is the pseudoactivation energy related to the motion of the polymer segments, and T_0 is the ideal glass transition temperature.[60] The fit with the VTF equation confirmed that the ionic motion in the GPEs was associated with free-volume transport and segmental motion within the polymer (see Supporting Information Figure S2).[61] Table S1 presents the parameters obtained from fitting. GPE-AVM exhibited a high carrier ion density (i.e., a high A value) and low temperature dependence in ion transport (i.e., a low E_0 value), which is most likely the result of high free-volume density. This confirms that the addition of PMMA to the PAV framework increased the interstitial space in the GPEs. However, the free volume might have provided space for solvent crystallization and elevated the glass transition temperature from −78 °C (205 K) for GPE-AV to −68 °C (195 K) for GPE-AVM. A comparison of data related to GPE and SLE led to the conclusion that the interaction with polymer chains substantially reduced the probability of solvent crystallization at low temperatures.

3.3. Electrochemical Stability of GPEs. We analyzed the electrochemical stability of the electrolytes using linear voltage scans. Figure 6 presents the voltammograms of cells assembled with the electrolytes inserted between an SS working electrode and a Li counter electrode. When anodic polarization was applied to the working electrode, the SLE cell exhibited an abrupt increase in current at approximately 5 V (vs Li/Li^+). The onset of anodic current flow was associated with the decomposition of electrolyte anions on the surface of the electrode.[62,63] GPE-AV and GPE-AVM cells exhibited far lower

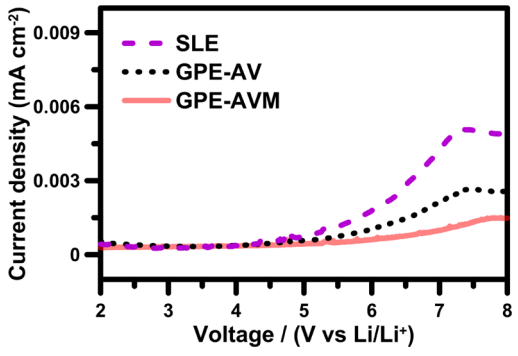

Figure 6. Linear scan voltammograms of cells assembled by inserting an electrolyte (GPE-AVM, GPE-AV or SLE) between a working stainless-steel electrode and a Li-metal counter electrode at 5 mV s^{-1}.

induced currents at an anodic voltage of 8 V (vs Li/Li$^+$). The results in Figure 6 indicate that the polymer chains stabilized the PF_6^- anions through the formation of $PF_6^-\cdots(\delta^+)C{\equiv}N(\delta^-)$ or $PF_6^-\cdots(\delta^+)C{=}O(\delta^-)$ complexes in the polymer framework. The stability window of the GPE-AVM cell was exceptionally wide, indicating how the addition of PMMA resulted in the segregation of polymer chains, which strengthened the interaction between PF_6^- and C≡N or C=O groups. The gradual current increase of the GPE-AVM cell induced by the applied anodic voltage may result from degradation of solvent molecules and polymer, as well as the PF_6^- anions. A wide stability window is highly beneficial to the application of GPEs in LIBs, particularly when using high-voltage cathode materials such as $LiCoMnO_4$, $Li_2NiMn_3O_8$, and $LiNi_{1/3}Mn_{1/3}Co_{1/3}O_2$.[64,65]

The transport of PF_6^- anions within the electrolytes polarizes the electrodes and induces ionic diffusion resistance.[62,63] A stationary anion (i.e., $t_{Li+} = 1$) can be beneficial to the elimination of polarization resistance. This study determined the electrolyte t_{Li+} value using a cell consisting of two Li-metal electrodes sandwiching SLE or GPEs. This analysis required polarizing the cell to a low DC voltage of 5 mV (V_{DC}) in order to obtain the initial and steady-state currents, I_0 and I_{ss}, respectively (Figure 7a). At the same time, AC impedance

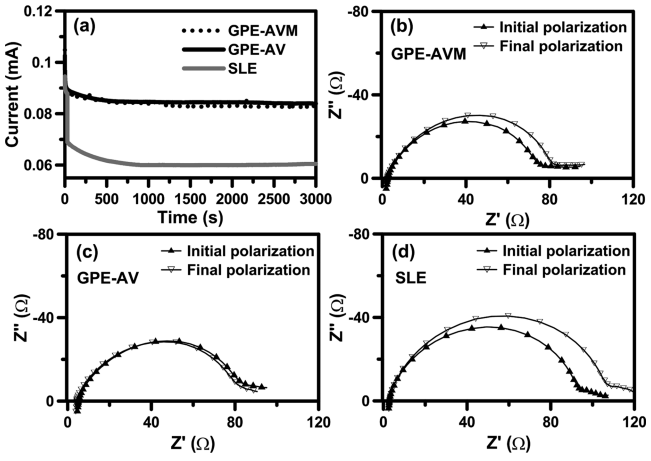

Figure 7. (a) Current−time curves of the Li|GPE-AVM|Li, Li|GPE-AV|Li, and Li|SLE|Li cells after applying a DC voltage of 5 mV to the cell. Corresponding Nyquist impedance plots of the cells for determining the initial and final R_{int} values: (b) GPE-AVM, (c) GPE-AV, (d) SLE.

analysis was used to simultaneously monitor the initial (0 mV) and steady-state (5 mV) resistances ($R_{int,0}$ and $R_{int,ss}$) associated with charge transfer at the Li-metal interfaces, as shown in Figure 7(b, c, and d).[66] The resulting parameters were then used to determine the t_{Li+} values, as follows:

$$t_{Li^+} = \frac{I_{ss}(\Delta V_{DC} - I_o R_{int,0})}{I_o(\Delta V_{DC} - I_{ss} R_{int,ss})} \quad (2)$$

The use of eq 2 resulted in t_{Li+} values of approximately 0.4, 0.5, and 0.6 for SLE, GPE-AV, and GPE-AVM, respectively. The high t_{Li^+} values of the GPEs may be due to segmental motion of polymer chains, which facilitated the transport of Li$^+$ ions in GPEs and the formation of $PF_6^-\cdots(\delta^+)C{-}C{\equiv}N(\delta^-)$ or $PF_6^-\cdots(\delta^+)C{-}C{=}O(\delta^-)$ complexes in the polymer matrices, resulting in the immobilization of the PF_6^- anion. Further segregating PAN chains with PMMA promoted the function of polymers with regard to Li$^+$ transport and PF_6^- fixation, which increased the t_{Li^+} value. A high t_{Li^+} value lowers electrode polarization resistance and also extends the lifespan of the cell by suppressing anion decomposition on the positive electrode.[67−69]

3.4. Electrolyte Performance in Full-Cell LIBs. This study used AC impedance spectroscopy to analyze the interfacial charge-transfer behavior in full-cell LIBs. The LIBs were assembled by sandwiching the electrolytes between a $LiFePO_4$ working electrode and a graphite counter electrode. Figure 8 presents the impedance complex-plane spectra of the

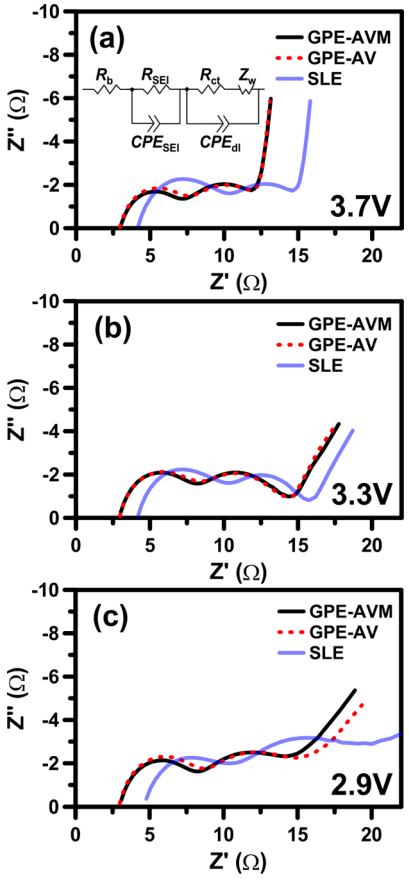

Figure 8. Nyquist impedance plots of the full-cell graphite|electrolyte|$LiFPO_4$ batteries obtained by applying varying voltages: (a) 3.7, (b) 3.3, and (c) 2.9 V. The inset of panel a shows the equivalent circuit simulating the impedance spectra.

graphite|electrolyte|$LiFePO_4$ batteries under various applied voltages. The spectra comprise two partially overlapped semicircles in the high frequency region and a sloping line in the low frequency region. The inset of Figure 8a presents an equivalent circuit that simulates bulk solution resistance (R_b), solid-electrolyte interphase (SEI) layer resistance (R_{SEI}), constant phase element of SEI (CPE_{SEI}), charge transfer resistance (R_{ct}), the constant phase element of the electric double layer (CPE_{dl}), and Warburg impedance (Z_w) in the cells. The first semicircle in the highest frequency region characterizes charge motion across the SEI layer and the remainder of the spectra corresponds to faradic impedance consisting of charge-transfer impedance (the second semicircle) and Warburg impedance (the sloping line). Faradic impedance is a reflection of the reaction kinetics within a cell, which varies

dx.doi.org/10.1021/am505448a | ACS Appl. Mater. Interfaces 2014, 6, 19360−19370

considerably according to the state of anode lithiation (i.e., applied voltage).[70]

Table 2 presents a summary of resistance-related data obtained from fitting the spectra to the equivalent circuit

Table 2. Resistance Data of the Full-Cell Graphite|Electrolyte|$LiFePO_4$ Batteries Obtained from Fitting the Impedance Spectra (Figure 8) to the Equivalent Circuit Shown in the Inset of Figure 8a

voltage (V)	R_b (Ω)	R_{SEI} (Ω)	R_{ct} (Ω)
	GPE-AVM		
3.7	2.9	4.4	3.9
3.3	2.9	4.9	6.2
2.9	2.9	5.1	6.1
	GPE-AV		
3.7	2.9	4.7	4.3
3.3	2.9	5.3	6.0
2.9	2.9	5.7	6.4
	SLE		
3.7	4.4	5.1	5.0
3.3	4.2	5.4	5.8
2.9	4.8	5.7	9.9

presented in the inset of Figure 8a. The R_b values, which did not vary with applied voltage, were lower in GPE cells than in SLE cells. As shown in Figure 5, the ionic conductivity values of GPEs are higher than those of SLE. The R_{SEI} value increased slightly with applied voltage, indicating that drift flow dominated ion motion in the SEI layer. The R_{ct} value corresponds to the reaction kinetics and is therefore expected to be highly voltage dependent. Figure 8 and Table 2 revealed a substantial decrease in the R_{ct} value when the anode reached a high lithiation level of 3.7 V. The R_{SEI} and R_{ct} values of the cells were both electrolyte dependent, in the following order GPE-PAVM < GPE-PAV < SLE. These results indicate that the larger t_{Li^+} values of GPEs associated with lower electrode polarization led to the formation of less charge motion resistance at the electrode interfaces.

Figure 9 presents the galvanostatic charge−discharge profiles of graphite|electrolyte|$LiFePO_4$ batteries, which were charged to 3.8 V at 0.1 C, whereupon they were discharged to 2.0 V at various C-rates. This study defined the battery C-rates according to the $LiFePO_4$ cathode under the assumption that the maximum achievable capacity was 155 mAh g^{-1} (determined using a half cell) for this full cell system. At low rates, all of the cells revealed plateaus in the charge and discharge voltage near 3.3 V, corresponding to the difference between the equilibrium potentials associated with the biphasic Li^+ extraction/insertion in the $LiFePO_4$ cathode and graphite anode. The voltage plateaus deviated from 3.3 V with an increase in the discharge rate. The deviation in voltage (ΔV) corresponds to the sum of the serial resistance and the polarization of the electrodes.[27] Figure 10 illustrates the variation in ΔV with the discharge rate of the batteries. We used the slope of the linear relationship to determine overall resistance, which produced values of 47, 65, and 77 Ω for GPE-AVM, GPE-AV, and SLE batteries, respectively. GPEs proved superior to SLE in facilitating ion motion in the batteries. Introducing PMMA into the PAV framework resulted in a substantial decrease (nearly 30%) in the overall resistance, indicating that segregating the PAN segments was a critical

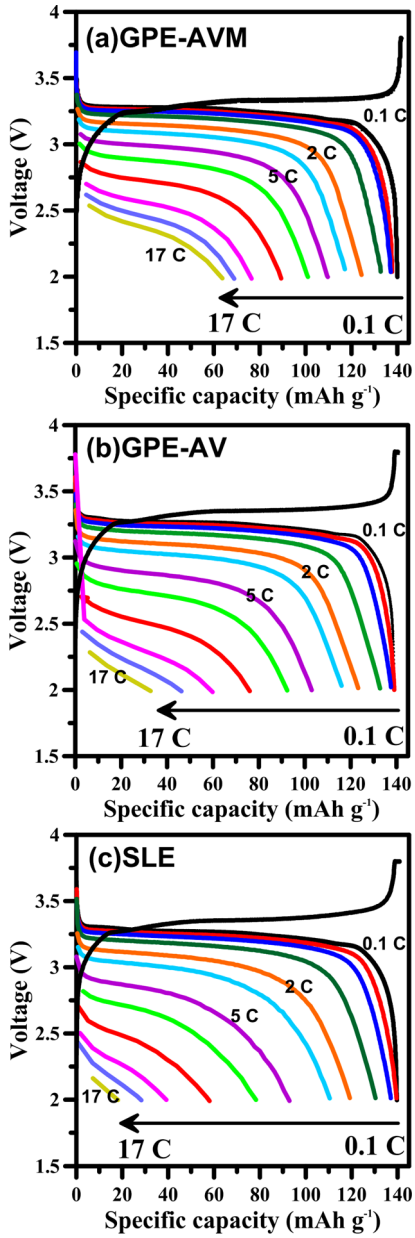

Figure 9. Galvanostatic charge−discharge profiles of the full-cell graphite|electrolyte|$LiFPO_4$ batteries charged at 0.1 C-rate and discharged at varying C-rates between 2.0 and 3.8 V: (a) graphite|GPE-AVM|$LiFPO_4$, (b) graphite|GPE-AV|$LiFPO_4$, and (c) graphite|SLE|$LiFPO_4$. This study defined the battery C-rates on the basis of the $LiFePO_4$ cathode by assuming a maximal achievable capacity of 155 mAh g^{-1} for this full-cell system.

tactic in facilitating the transport of ions and increasing the t_{Li^+} value in order to lower polarization resistance at the electrodes.

Differences in the overall resistance influenced the performance of the batteries. Table 3 summarizes the capacities of the batteries discharged at various C-rates, based on the data in Figure 9. All of the batteries presented similar capacities of ∼140 mAh g^{-1} at 0.1 C; however, differences in battery capacity became prominent at discharge rates exceeding 3 C. The SLE battery has a capacity of 110 mAh g^{-1} at 3 C, whereas the capacity of GPE batteries exceeded this value. A further increase in C-value caused differences in capacity for the two GPE batteries. The GPE-AVM battery produced a high discharge capacity of 67 mAh g^{-1} at 17 C, which corresponds

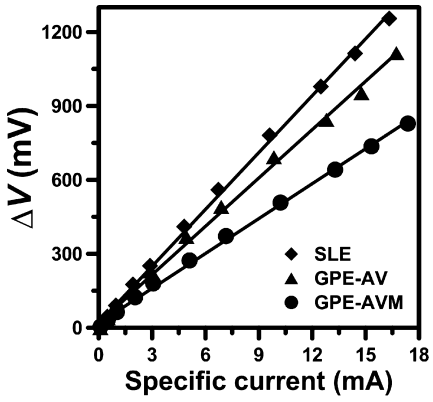

Figure 10. Deviation of the discharge voltage plateaus from the equilibrium state, 3.3 V, (i.e., ΔV) as a function of the discharge current for the graphite|electrolyte|$LiFePO_4$ batteries using the GPE-AVM, GPE-AV, and SLE electrolytes. The ΔV value corresponds to the sum of the battery's IR drop resulting from the serial resistance and the polarization of the electrodes.

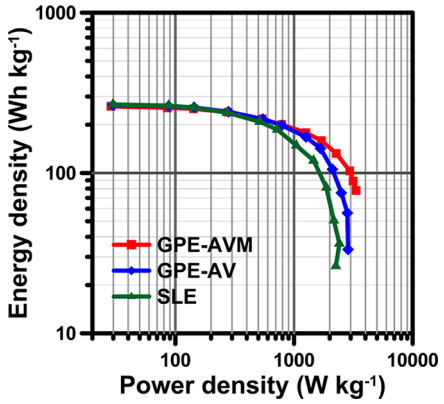

Figure 11. Ragone plots of the graphite|electrolyte|$LiFePO_4$ batteries using the GPE-AVM, GPE-AV, and SLE electrolytes. Data obtained from the galvanostatic discharge measurement at various C-rates.

to 48% of the retention capacity obtained at 0.1 C. GPE-AV and SLE batteries produced only 33 and 18 mAh g^{-1} (or 24% and 13% retention), respectively. Figures 9 and 10 illustrate the significant influence of the electrolyte host on battery power delivery, which is related to the capacity retention, as well as the preservation of energy according to the ΔV value of the battery.

Ragone plots of a full-cell battery are correlated with the specific power and energy of the device, thereby providing a more comprehensive indication of battery performance. This study used galvanostatic discharge data (Figure 9) to correlate the specific power and energy of the graphite|electrolyte|$LiFePO_4$ batteries

$$E = \frac{\int IV \, dt}{M} \tag{3}$$

$$P = \frac{E}{t_d} \tag{4}$$

where E and P are specific energy and power, respectively, I is the discharge current, V is the voltage value in discharge, M is the total mass of the active materials in the cathode and anode (not including the binder and carbon black), and t_d is the time required for complete discharge. Figure 11 reveals the correlation between E and P in the Ragone plots. All of the batteries attained energy values exceeding 260 Wh kg^{-1}. GPEs were superior to SLE in the preservation of energy at high power values. The presence of PMMA in the polymer framework substantially improved the power performance of the LIBs. In the delivery of energy at 100 Wh kg^{-1}, the power rate of the GPE-AVM battery reached 2.9 kW kg^{-1}, whereas the power rates of GPE-AV and SLE batteries were 2.1 and 1.4 kW kg^{-1}, respectively. Because of its superior ability to preserve energy at high power rates, GPE-AVM must have robust electrode/electrolyte interfaces and can be expected to have a long cycle life.

Figure 12 presents the charge and discharge capacities of the GPE-AVM battery as a function of the number of galvanostatic cycles at a high rate of 17 C. This battery presented capacity retention of 93% after 100 cycles and 63% after 1000 cycles. The SLE battery retained only 42% of the original capacity after 100 cycles (see Figure S3 of the Supporting Information). Figure 12 also reveals that the Coulombic efficiency, which is defined as the capacity ratio of discharge to charge, was maintained at 100% throughout the cycling process. This high Coulombic efficiency reflects the high charge transfer reversibility of the GPE-AVM battery.

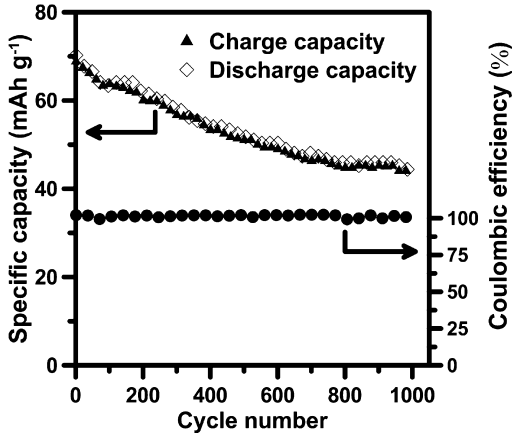

Figure 12. Charge and discharge capacities and the Coulombic efficiencies of the full-cell graphite|GPE-AVM|$LiFePO_4$ batteries as a function of cycle number at 17 C-rate with a voltage range between 2.0 and 3.8 V.

Table 3. Discharge Capacities of the Full-Cell Graphite|Electrolyte|$LiFePO_4$ Batteries Operating at Various C-Rates Based on the Data in Figure 9

	C-rate								
electrolyte	0.1	0.5	1	3	5	7	10	13	17
GPE-AVM	140	137	133	118	110	101	89	76	67
GPE-AV	139	137	133	116	103	92	76	60	33
SLE	139	137	131	110	93	78	58	39	18

dx.doi.org/10.1021/am505448a | ACS Appl. Mater. Interfaces 2014, 6, 19360−19370

4. SUMMARY AND CONCLUSIONS

This study developed PAN-based polymer hosts for GPEs to enable LIBs to achieve high rates and long cycle-life performance. The PAV framework derived through the linear conjugation of PAN with PVAc exhibited high LE-accommodating capacity and mechanical strength. Integrating PMMA within PAV for the segregation of PAN chains was shown to enhance the LE-accommodating capacity of the resulting PAVM. GPEs derived by soaking electrospun PAV and PAVM in LE solution (i.e., GPE-AV and GPE-AVM) exhibited higher ionic conductivity values compared to SLE coming from LE swelling a commercial separator membrane. The electrochemical stability and t_{Li^+} value of the electrolytes were in the following order: GPE-AVM > GPE-AV > SLE. This can be attributed primarily to the strong binding between electrolyte anions and segregated PAV chains. GPE-AVM had a high t_{Li^+} value of 0.6; therefore, full-cell graphite|GPE-AVM|$LiFePO_4$ batteries presented lower R_{SEI} and R_{ct} values compared to batteries assembled with SLE or GPE-AV. The Graphite|GPE-AVM|$LiFePO_4$ battery presented a discharge capacity of 140 and 67 mAh g^{-1} at 0.1 and 17 C, respectively. The battery also presented a specific power 2.1 times that of the graphite|SLE|$LiFePO_4$ battery in the delivery of energy at 100 Wh kg^{-1} and reduced resistance in the battery by 39%. The robustness of interfaces in the GPE-AVM batteries resulted in a long cycle life at high charge−discharge rates (93% capacity retention for 100 cycles and 63% for 1000 cycles at 17 C). This paper demonstrates how PAN-based GPE hosts of high mechanical and chemical stability can be produced using PVAc and PMMA chains.

■ ASSOCIATED CONTENT

Ⓢ Supporting Information

Impedance data of the GPE-AVM, GPE-AV, and SLE electrolytes at varying temperatures, the fit to the VTF equation for the temperature dependence of electrolyte conductivity, and the variation of capacity with operation cycle for the SLE battery. This material is available free of charge via the Internet at http://pubs.acs.org.

■ AUTHOR INFORMATION

Corresponding Authors

*E-mail: hteng@mail.ncku.edu.tw. Fax: 886-6-2344496. Tel: 886-6-2385371.

*E-mail: cthsieh@saturn.yzu.edu.tw.

Notes

The authors declare no competing financial interest.

■ ACKNOWLEDGMENTS

This research was supported by the Ministry of Science and Technology, Taiwan (101-2221-E-006-243-MY3, 101-2221-E-006-225-MY3, 103-3113-E-006-009, and 102-3113-E-006-002), and by the Ministry of Education, Taiwan, The Aim for the Top University Project to the National Cheng Kung University.

■ REFERENCES

(1) Scrosati, B.; Hassoun, J.; Sun, Y. K. Lithium-Ion Batteries. A Look into the Future. *Energy Environ. Sci.* **2011**, *4*, 3287−3295.

(2) Hwang, S. S.; Cho, C. G.; Kim, H. Room Temperature Cross-Linkable Gel Polymer Electrolytes for Lithium Ion Batteries by In Situ Cationic Polymerization of Divinyl Ether. *Electrochem. Commun.* **2010**, *12*, 916−919.

(3) Yang, C. M.; Kim, H. S.; Na, B. K.; Kum, K. S.; Cho, B. W. Gel-Type Polymer Electrolytes with Different Types of Ceramic Fillers and Lithium Salts for Lithium-Ion Polymer Batteries. *J. Power Sources* **2006**, *156*, 574−580.

(4) Li, H.; Chen, Y. M.; Ma, X. T.; Shi, J. L.; Zhu, B. K.; Zhu, L. P. Gel Polymer Electrolytes Based on Active PVDF Separator for Lithium Ion Battery. I: Preparation and Property of PVDF/Poly(Dimethylsiloxane) Blending Membrane. *J. Membr. Sci.* **2011**, *379*, 397−402.

(5) Wang, X. L.; Cai, Q.; Fan, L. Z.; Hua, T.; Lin, Y. H.; Nan, C. W. Gel-Based Composite Polymer Electrolytes with Novel Hierarchical Mesoporous Silica Network for Lithium Batteries. *Electrochim. Acta* **2008**, *53*, 8001−8007.

(6) Pandey, G. P.; Agrawal, R. C.; Hashmi, S. A. Magnesium Ion-Conducting Gel Polymer Electrolytes Dispersed with Nanosized Magnesium Oxide. *J. Power Sources* **2009**, *190*, 563−572.

(7) Ferrari, S.; Quartarone, E.; Mustarelli, P.; Magistris, A.; Fagnoni, M.; Protti, S.; Gerbaldi, C.; Spinella, A. Lithium Ion Conducting PVdF−HFP Composite Gel Electrolytes Based on *N*-Methoxyethyl-*N*-methylpyrrolidinium Bis(Trifluoromethanesulfonyl)-imide Ionic Liquid. *J. Power Sources* **2010**, *195*, 559−566.

(8) Wu, N.; Cao, Q.; Wang, X.; Li, X.; Deng, H. A Novel High-Performance Gel Polymer Electrolyte Membrane Basing on Electrospinning Technique for Lithium Rechargeable Batteries. *J. Power Sources* **2011**, *196*, 8638−8643.

(9) Raghavan, P.; Manuel, J.; Zhao, X.; Kim, D. S.; Ahn, J. H.; Nah, C. Preparation and Electrochemical Characterization of Gel Polymer Electrolyte Based on Electrospun Polyacrylonitrile Nonwoven Membranes for Lithium Batteries. *J. Power Sources* **2011**, *196*, 6742−6749.

(10) Kumar, D.; Hashmi, S. A. Ion Transport and Ion−Filler−Polymer Interaction in Poly(Methyl Methacrylate)-Based, Sodium Ion Conducting, Gel Polymer Electrolytes Dispersed with Silica Nanoparticles. *J. Power Sources* **2010**, *195*, 5101−5108.

(11) Wang, Y.; Ma, X.; Zhang, Q.; Tian, N. Synthesis and Properties of Gel Polymer Electrolyte Membranes Based on Novel Comb-like Methyl Methacrylate Copolymers. *J. Membr. Sci.* **2010**, *349*, 279−286.

(12) Jung, H. R.; Lee, W. J. Electrochemical Characteristics of Electrospun Poly(Methyl Methacrylate)/Polyvinyl Chloride as Gel Polymer Electrolytes for Lithium Ion Battery. *Electrochim. Acta* **2011**, *58*, 674−680.

(13) Rajendran, S.; Prabhu, M. R.; Rani, M. U. Ionic Conduction in Poly(Vinyl Chloride)/Poly(Ethyl Methacrylate)-Based Polymer Blend Electrolytes Complexed with Different Lithium Salts. *J. Power Sources* **2008**, *180*, 880−883.

(14) Wang, Q.; Song, W. Li.; Wang, L.; Song, Y.; Shi, Q.; Fan, L. Z. Electrospun Polyimide-Based Fiber Membranes as Polymer Electrolytes for Lithium-Ion Batteries. *Electrochim. Acta* **2014**, *132*, 538−544.

(15) Carol, P.; Ramakrishnan, P.; John, B.; Cheruvally, G. Preparation and Characterization of Electrospun Poly(Acrylonitrile) Fibrous Membrane Based Gel Polymer Electrolytes for Lithium-Ion Batteries. *J. Power Sources* **2011**, *196*, 10156−10162.

(16) Croce, F.; Focarete, M. L.; Hassoun, J.; Meschini, I.; Scrosati, B. A Safe, High-Rate and High-Energy Polymer Lithium-Ion Battery Based on Gelled Membranes Prepared by Electrospinning. *Energy Environ. Sci.* **2011**, *4*, 921−927.

(17) Jeong, H. S.; Choi, E. S.; Lee, S. Y. Composition Ratio-Dependent Structural Evolution of SiO_2/Poly(Vinylidene Fluoride-hexafluoropropylene)-Coated Poly(Ethylene Terephthalate) Nonwoven Composite Separators for Lithium-Ion Batteries. *Electrochim. Acta* **2012**, *86*, 317−322.

(18) Xiao, Q.; Li, Z.; Gao, D.; He, T.; Zhang, H. Preparation and Electrochemical Performance of Gel Polymer Electrolytes with a Novel Star Network. *J. Appl. Electrochem.* **2009**, *39*, 247−251.

(19) Chen, Z. H.; Zhang, L. Z.; West, R.; Amine, K. Gel Electrolyte for Lithium-Ion Batteries. *Electrochim. Acta* **2008**, *53*, 3262−3266.

(20) Isken, P.; Winter, M.; Passerini, S.; Balducci, A. L. Methacrylate Based Gel Polymer Electrolyte for Lithium-Ion Batteries. *J. Power Sources* **2013**, *225*, 157−162.

(21) Wang, F. M.; Lee, J. T.; Cheng, J. H.; Cheng, C. S.; Yang, C. R. The Network Gel Polymer Electrolyte Based on Poly(Acrylate-co-imide) and Its Transport Properties in Lithium Ion Batteries. *J. Solid State Electrochem.* **2009**, *13*, 1425−1431.
(22) Zhou, D.; Fan, L. Z.; Fan, H.; Shi, Q. Electrochemical Performance of Trimethylolpropane Trimethylacrylate-Based Gel Polymer Electrolyte Prepared by In Situ Thermal Polymerization. *Electrochim. Acta* **2013**, *89*, 334−338.
(23) Oh, S.; Kim, D. W.; Lee, C.; Lee, M. H.; Kang, Y. Poly(Vinylpyridine-co-styrene) Based In Situ Cross-Linked Gel Polymer Electrolyte for Lithium-Ion Polymer Batteries. *Electrochim. Acta* **2011**, *57*, 46−51.
(24) Park, J. H.; Kim, J. S.; Shim, E. G.; Lee, S. Y. Polyimide Gel Polymer Electrolyte-Nanoencapsulated $LiCoO_2$ Cathode Materials for High-Voltage Li-Ion Batteries. *Electrochem. Commun.* **2010**, *12*, 1099−1102.
(25) Park, J. H.; Cho, J. H.; Kim, J. S.; Shim, E. G.; Lee, S. Y. High-Voltage Cell Performance and Thermal Stability of Nanoarchitectured Polyimide Gel Polymer Electrolyte-Coated $LiCoO_2$ Cathode Materials. *Electrochim. Acta* **2012**, *86*, 346−351.
(26) Park, J. H.; Cho, J. H.; Lee, E. H.; Kim, J. M.; Lee, S. Y. Thickness-Tunable Polyimide Nanoencapsulating Layers and Their Influence on Cell Performance/Thermal Stability of High-Voltage $LiCoO_2$ Cathode Materials for Lithium-Ion Batteries. *J. Power Sources* **2013**, *244*, 442−449.
(27) Huang, L. Y.; Shih, Y. C.; Wang, S. H.; Kuo, P. L.; Teng, H. Gel Electrolytes Based on an Ether-Abundant Polymeric Framework for High-Rate and Long-Cycle-Life Lithium Ion Batteries. *J. Mater. Chem. A* **2014**, *2*, 10492−10501.
(28) Wang, S. H.; Hou, S. S.; Kuo, P. L.; Teng, H. Poly(Ethylene Oxide)-co-poly(propylene oxide)-Based Gel Electrolyte with High Ionic Conductivity and Mechanical Integrity for Lithium-Ion Batteries. *ACS Appl. Mater. Interfaces* **2013**, *5*, 8477−8485.
(29) Cao, J.; Wang, L.; Fang, M.; Shang, Y.; Deng, L.; Yang, J.; Li, J.; Chen, H.; He, X. Interfacial Compatibility of Gel Polymer Electrolyte and Electrode on Performance of Li-Ion Battery. *Electrochim. Acta* **2013**, *114*, 527−532.
(30) Stephan, A. M.; Nahm, K. S. Review on Composite Polymer Electrolytes for Lithium Batteries. *Polymer* **2006**, *47*, 5952−5964.
(31) Akashi, H.; Sekai, K.; Tanaka, K. A Novel Fire-Retardant Polyacrylonitrile-Based Gel Electrolyte for Lithium Batteries. *Electrochim. Acta* **1998**, *43*, 1193−1197.
(32) Park, J. H.; Cho, J. H.; Lee, E. H.; Kim, J. M.; Lee, S. Y. Conductivity Enhancement of Polyacrylonitrile-Based Electrolytes by Addition of Cascade Nitrile Compounds. *J. Power Sources* **2000**, *90*, 33−38.
(33) Abraham, K. M.; Alamgir, M. Li^+-Conductive Solid Polymer Electrolytes with Liquid-Like Conductivity. *J. Electrochem. Soc.* **1990**, *137*, 1657−1658.
(34) Huq, R.; Koksbang, R.; Tonder, P. E.; Farrington, G. C. Effect of Plasticizers on the Properties of New Ambient Temperature Polymer Electrolyte. *Electrochim. Acta* **1992**, *37*, 1681−1684.
(35) Wu, G.; Yang, H. Y.; Chen, H. Z.; Yuan, F.; Yang, L. G.; Wang, M.; Fu, R. J. Novel Porous Polymer Electrolyte Based on Polyacrylonitrile. *Mater. Chem. Phys.* **2007**, *104*, 284−287.
(36) Raghavan, P.; Zhao, X.; Shin, C.; Baek, D. H.; Choi, J. W.; Manuel, J.; Heo, M. Y.; Ahn, J. H.; Nah, C. Preparation and Electrochemical Characterization of Polymer Electrolytes Based on Electrospun Poly(Vinylidene Fluoride-co-hexafluoropropylene)/Polyacrylonitrile Blend/Composite Membranes for Lithium Batteries. *J. Power Sources* **2010**, *195*, 6088−6094.
(37) Amaral, F. A.; Dalmolin, C.; Canobre, S. C.; Bocchi, N.; Rocha-Filho, R. C.; Biaggio, S. R. Electrochemical and Physical Properties of Poly(Acrylonitrile)/Poly(Vinyl Acetate)-Based Gel Electrolytes for Lithium Ion Batteries. *J. Power Sources* **2007**, *164*, 379−385.
(38) Baskaran, R.; Selvasekarapandian, S.; Kuwata, N.; Kawamura, J.; Hattori, T. Structure, Thermal and Transport Properties of PVAc−$LiClO_4$ Solid Polymer Electrolytes. *J. Phys. Chem. Solids* **2007**, *68*, 407−412.
(39) Stephan, A. M.; Renganathan, N. G.; Kumar, T. P.; Thirunakaran, R.; Pitchumani, S.; Shrisudersan, J.; Muniyandi, N. Ionic Conductivity Studies on Plasticized PVC/PMMA Blend Polymer Electrolyte Containing $LiBF_4$ and $LiCF_3SO_3$. *Solid State Ionics* **2000**, *130*, 123−132.
(40) Appetecchi, G. B.; Croce, F.; Scrosati, B. Kinetics and Stability of the Lithium Electrode in Poly(Methylmethacrylate)-Based Gel Electrolytes. *Electrochim. Acta* **1995**, *40*, 991−997.
(41) Liao, Y.; Rao, M.; Li, W.; Tan, C.; Yi, J.; Chen, L. Improvement in Ionic Conductivity of Self-Supported P(MMA-AN-VAc) Gel Electrolyte by Fumed Silica for Lithium Ion Batteries. *Electrochim. Acta* **2009**, *54*, 6396−6402.
(42) Tu, C. W.; Liu, K. Y.; Chien, A. T.; Lee, C. H.; Ho, K. C.; Lin, K. F. Performance of Gelled-Type Dye-Sensitized Solar Cells Associated with Glass Transition Temperature of the Gelatinizing Polymers. *Eur. Polym. J.* **2008**, *44*, 608−614.
(43) Choi, S. W.; Kim, J. R.; Jo, S. M.; Lee, W. S.; Kim, Y. R. Electrochemical and Spectroscopic Properties of Electrospun PAN-Based Fibrous Polymer Electrolytes Batteries, Fuel Cells, and Energy Conversion. *J. Electrochem. Soc.* **2005**, *152*, A989−A995.
(44) Mohamed, S. N.; Johari, N. A.; Ali, A. M. M.; Harun, M. K.; Yahya, M. Z. A. Electrochemical Studies on Epoxidised Natural Rubber-Based Gel Polymer Electrolytes for Lithium−Air Cells. *J. Power Sources* **2008**, *183*, 351−354.
(45) Aroca, R.; Nazri, M.; Nazri, G. A.; Camargo, A. J.; Trsic, M. Vibrational Spectra and Ion-Pair Properties of Lithium Hexafluorophosphate in Ethylene Carbonate Based Mixed-Solvent Systems for Lithium Batteries. *J. Solution Chem.* **2000**, *29*, 1047−1060.
(46) Kondo, K.; Sano, M.; Hiwara, A.; Omi, T.; Fujita, M.; Kuwae, A.; Iida, M.; Mogi, K.; Yokoyama, H. Conductivity and Solvation of Li^+ Ions of $LiPF_6$ in Propylene Carbonate Solutions. *J. Phys. Chem. B* **2000**, *104*, 5040−5044.
(47) Burba, C. M.; Frech, R. Spectroscopic Measurements of Ionic Association in Solutions of $LiPF_6$. *J. Phys. Chem. B* **2005**, *109*, 15161−15164.
(48) Wang, Z.; Huang, B.; Wang, S.; Xue, R.; Huang, X.; Chen, L. Competition Between the Plasticizer and Polymer on Associating with Li^+ Ions in Polyacrylonitrile-Based Electrolytes. *J. Electrochem. Soc.* **1997**, *144*, 778−786.
(49) Wang, Z.; Huang, B.; Xue, R.; Huang, X.; Chen, L. Spectroscopic Investigation of Interactions among Components and Ion Transport Mechanism in Polyacrylonitrile Based Electrolytes. *Solid State Ionics* **1999**, *121*, 141−156.
(50) Kuo, P. L.; Liang, W. J.; Chen, T. Y. Solid Polymer Electrolytes V: Microstructure and Ionic Conductivity of Epoxide-Crosslinked Polyether Networks Doped with $LiClO_4$. *Polymer* **2003**, *44*, 2957−2964.
(51) Rajendran, S.; Uma, T. Lithium Ion Conduction in PVC−$LiBF_4$ Electrolytes Gelled with PMMA. *J. Power Sources* **2000**, *88*, 282−285.
(52) Saunier, J.; Alloin, F.; Sanchez, J. Y.; Caillon, G. Thin and Flexible Lithium-Ion Batteries: Investigation of Polymer Electrolytes. *J. Power Sources* **2003**, *119*−*121*, 454−459.
(53) Arora, P.; Zhang, Z. Battery Separators. *Chem. Rev.* **2004**, *104*, 4419−4462.
(54) Liang, W. J.; Chen, T. Y.; Kuo, P. L. Solid Polymer Electrolytes. VII. Preparation and Ionic Conductivity of Gelled Polymer Electrolytes Based on Poly(Ethylene Glycol) Diglycidyl Ether Cured with α,ω-Diamino Poly(Propylene Oxide). *J. Appl. Polym. Sci.* **2004**, *92*, 1264−1270.
(55) Tien, C. P.; Liang, W. J.; Kuo, P. L.; Teng, H. Electric Double Layer Capacitors with Gelled Polymer Electrolytes Based on Poly(Ethylene Oxide) Cured with Poly(Propylene Oxide) Diamines. *Electrochim. Acta* **2008**, *53*, 4505−4511.
(56) Rajendran, S.; Babu, R. S.; Sivakumar, P. Effect of Salt Concentration on Poly(Vinyl Chloride)/Poly(Acrylonitrile) Based Hybrid Polymer Electrolytes. *J. Power Sources* **2007**, *170*, 460−464.
(57) Baskaran, R.; Selvasekarapandian, S.; Kuwata, N.; Kawamura, J.; Hattori, T. Conductivity and Thermal Studies of Blend Polymer

Electrolytes Based on PVAc−PMMA. *Solid State Ionics* **2006**, *177*, 2679−2682.
(58) Xiao, Q.; Wang, X.; Li, W.; Li, Z.; Zhang, T.; Zhang, H. Macroporous Polymer Electrolytes Based on PVDF/PEO-b-PMMA Block Copolymer Blends for Rechargeable Lithium Ion Battery. *J. Membr. Sci.* **2009**, *334*, 117−122.
(59) Gopalan, A. I.; Santhosh, P.; Manesh, K. M.; Nho, J. H.; Kim, S. H.; Hwang, C. G.; Lee, K. P. Development of Electrospun PVdF−PAN Membrane-Based Polymer Electrolytes for Lithium Batteries. *J. Membr. Sci.* **2008**, *325*, 683−690.
(60) Ryou, M. H.; Lee, Y. M.; Cho, K. Y.; Han, G. B.; Lee, J. N.; Lee, D. J.; Choi, J. W.; Park, J. K. A Gel Polymer Electrolyte Based on Initiator-Free Photopolymerization for Lithium Secondary Batteries. *Electrochim. Acta* **2012**, *60*, 23−30.
(61) Pas, S. J.; Ingram, M. D.; Funke, K.; Hill, A. J. Free Volume and Conductivity in Polymer Electrolytes. *Electrochim. Acta* **2005**, *50*, 3955−3962.
(62) Park, C. H.; Kim, D. W.; Prakash, J.; Sun, Y. K. Electrochemical Stability and Conductivity Enhancement of Composite Polymer Electrolytes. *Solid State Ionics* **2003**, *159*, 111−119.
(63) Armand, M. M. In *Polymer Electrolyte Reviews*; MacCallum, J. R., Vincent, C. A., Eds.; Elsevier: London, 1987; Vol. *1*, pp 1−22.
(64) Kraytsberg, A.; Ein-Eli, Y. Higher, Stronger, Better... A Review of 5 V Cathode Materials for Advanced Lithium-Ion Batteries. *Adv. Energy Mater.* **2012**, *2*, 922−939.
(65) Chikkannanavar, S. B.; Bernardi, D. M.; Liu, L. A Review of Blended Cathode Materials for Use in Li-Ion Batteries. *J. Power Sources* **2014**, *248*, 91−100.
(66) Evans, J.; Vincent, C. A.; Bruce, P. G. Electrochemical Measurement of Transference Numbers in Polymer Electrolytes. *Polymer* **1987**, *28*, 2324−2328.
(67) Dias, F. B.; Plomp, L.; Veldhuis, J. B. J. Trends in Polymer Electrolytes for Secondary Lithium Batteries. *J. Power Sources* **2000**, *88*, 169−191.
(68) Sumathipala, H. H.; Hassoun, J.; Panero, S.; Scrosati, B. Li-$LiFePO_4$ Rechargeable Polymer Battery Using Dual Composite Polymer Electrolytes. *J. Appl. Electrochem.* **2008**, *38*, 39−42.
(69) Doyle, M.; Fuller, T. F.; Newman, J. The Importance of the Lithium Ion Transference Number in Lithium/Polymer Cells. *Electrochim. Acta* **1994**, *39*, 2073−2081.
(70) Song, J. Y.; Lee, H. H.; Wang, Y. Y.; Wan, C. C. Two- and Three-Electrode Impedance Spectroscopy of Lithium-Ion Batteries. *J. Power Sources* **2002**, *111*, 255−267.